Advances in Science and Technology Research Journal

Advances in Science and Technology Research Journal, 2026, 20(4), 227–240
https://doi.org/10.12913/22998624/214943
ISSN 2299-8624, License CC-BY 4.0

Received: 2025.09.06
Accepted: 2026.02.15
Published: 2026.03.01

Microstructural characterization and corrosion behavior of in-situ composites A356/Al_3Ni used in a 3.5 wt% NaCl solution

Noor Alhuda Baheer[1], Muna Khethier Abbass[2*], Israa Abd Al-Kadir Aziz[1]

[1] College of Production Engineering and Metallurgy, University of Technology, Baghdad, Iraq
[2] Ministry of Higher Education and Scientific Research, University of Technology, Baghdad, Iraq
* Corresponding author's e-mail: muna.k.abbass@uotechnology.edu.iq

ABSTRACT

Recent investigations have increasingly concentrated on the advancement of the in-situ technique with the objective of enhancing the wettability, uniformity, and thermodynamic stability of reinforcement particles within the aluminum matrix. In this study, stir casting was employed to fabricate in-situ composites based on Al alloy A356 reinforced with the Al_3Ni phase, incorporating different weight fractions of pure Ni powder (5 wt%, 10 wt%, and 15 wt%). Several evaluations, including microhardness measurements, microstructural analysis, and corrosion assessments, were conducted on the developed in-situ composites. The microstructural characteristics of Al alloy A356 revealed the formation of the in-situ Al_3Ni intermetallic phase within the matrix, along with a notable refinement of the A356 aluminum matrix. The hightlight findings indicated that the presence of the Al_3Ni particles enhanced both hardness and resistance to corrosion; consequently, the in-situ composite with 15 wt% Ni exhibited the maximum hardness value (152 HV) compared with the base alloy hardness (76 HV). A pronounced improvement in corrosion resistance was particularly evident in the composites containing 5 wt% Ni. It was shown that the 5% Ni composite exhibited the best corrosion resistance (97% improvement), as compared to the base alloy and other composites, which decreases with increasing Ni particles.

Keywords: A356 alloy, Al-alloy, Al_3Ni, corrosion rate, in-situ composite, microstructure, stir casting.

INTRODUCTION

The distinctive characteristics of metal matrix composites (MMC) have enabled their application in both the aerospace sector and the automotive industry. These materials exhibit elevated strength, a high elastic modulus, and notable resistance to abrasion and creep, while displaying limited fracture toughness and reduced flexibility as a result of the incorporated ceramic particles [1]. The term aluminum matrix composites (AMCs) refers to a specifically engineered combination of aluminum (matrix) with either matrix or rigid reinforcement (the matrix contains the reinforcing material). Numerous manufacturing processes have continuously evolved to improve the microstructure and mechanical characteristics of AMCs. Since the manufacturing process directly impacts the properties of the finished product, it is an essential part of creating AMCs. Solid- and liquid-state fabrications as well as in-situ-state fabrication are all included in the general category of ex-situ fabrication techniques for AMCs [2].

Aluminum-silicon (Al-Si) castings represent the most widely utilized type due to their engineering importance, acceptable mechanical performance, favorable resistance to corrosion, comparatively low coefficient of thermal expansion, as well as high fluidity during the melting and casting processes. For this reason, these alloys are frequently employed in various tribological and bearing applications [3]. Typical applications of the A356 alloy include aircraft pump components, automotive transmission housings, aircraft fittings, control parts, and water-cooled cylinder blocks. Additional utilization arises in the situations that demand excellent castability, reliable

weldability, pressure tightness, and strong resistance to corrosion. Furthermore, A356 is employed in aircraft structures, engine control systems, nuclear energy facilities, and other areas where permanent mold or investment castings with high strength are essential [4]. The fabrication techniques available for MMC can generally be divided into three main categories. These include solid-state processes, such as powder metallurgy and diffusion bonding; liquid-phase processes, such as stir casting and infiltration of the molten matrix into reinforcements; and semi-solid methods, including spray casting, Rheo casting, and Compo casting [5]. Among these, the stir casting technique offers several benefits compared with alternative processing methods, including operational simplicity, adaptability, applicability across a broad range of materials, cost-effectiveness, and a high production rate capable of producing large composite sizes [6]. A mechanical stirrer is utilized in stir casting, a type of casting approach, to mix reinforcement by causing a vortex in the matrix material. The key benefits of stir casting are its ease of use, adaptability, and potential for high volume production [7].

Additionally, an emerging in-situ processing route has gained attention, in which reinforcement forms within the matrix through reactions between one or more components and the matrix. These reinforcements exhibit extremely high melting points along with favorable mechanical characteristics [8]. The in-situ process consists of a chemical reaction that produces very fine, thermodynamically stable ceramic reinforcements with clean surfaces inside the metal matrix. The in-situ approach offers further benefits such as isotropic behavior, robust chemical interaction between the reinforcement and the matrix phase, and a consistent dispersion of reinforcement particles within the metal matrix [9].

Gobalakrishnan et al. [10] synthesized in-situ Al/TiB_2 MMC and ex-situ Al/SiC MMC through the stir casting technique by incorporating ceramic particulates in varying weight fractions of 2, 4, 6, and 8 wt%. The mechanical properties showed improvement as the reinforcement content increased from 2 to 8 wt%. The in-situ TiB_2 MMC demonstrates enhanced mechanical characteristics, including tensile strength, 0.2% proof strength, and hardness, when compared with both the base alloy and the ex-situ SiC MMC. Manjunatha et al. (2020) [11] produced the Al 6061-Mg-TiB_2 composite materials intended for lightweight applications through the in-situ salt reaction stir casting method by altering the TiB_2 content at 0, 3, 6, 9, and 12 wt%. The developed composites displayed superior properties relative to the matrix alloy.

Abu-Warda et al. [12] studied the A6005 aluminum alloy reinforced with 5 wt% nano-TiB_2, processed by mechanical alloying (MA) and hot extrusion. The MA process plus TiB_2 addition increased microhardness by 61%. Electrochemical tests in a NaCl solution showed that MA slightly improved corrosion resistance due to an amorphous Al_2O_3 passive layer, while TiB_2 had little effect. Both reinforced and unreinforced samples had similar corrosion current, and pitting mainly occurred at the Al_2O_3/aluminum interface.

Chandrashekar et al. [13] developed a composite by combining the B_4C particles of two distinct sizes with A356 aluminum alloy, followed by thorough stirring of the mixture. The three composite formulations included the A356 reinforced with 4% B_4C in a 3:1 ratio, 2% B_4C (44 µm and 105 µm particles in a 1:1 ratio), and 6% B_4C in a 1:3 ratio. The findings showed that the B_4C particles were dispersed uniformly throughout the alloy matrix. As a rule, higher concentrations of B_4C powders resulted in higher hardness and tensile strengths. Instead of deboning, tensile fractography revealed intercrystalline fractures, which manifested as particle breakage in B_4C.

Nawal and Abrar [14] studied the mechanical properties and corrosion resistance of aluminum by reinforcing it with yttrium oxide (Y_2O_3) and nickel (Ni) using the stir casting vortex method. The composite was formulated with a fixed 20% Ni content, while Y_2O_3 was varied from 3% to 9% by weight. Results indicated that hardness improved significantly, with a maximum increase of 52% upon the addition of 9% Y_2O_3. Corrosion behavior was evaluated in a 3.5 wt.% NaCl solution using potentiostatic polarization tests. The presence of nickel enhanced corrosion resistance compared to the base aluminum alloy. Furthermore, increasing the Y_2O_3 content reduced corrosion rates, with the lowest rate recorded at 6% Y_2O_3 (5.51 mpy)—a substantial improvement over the rate of 118.59 mpy exhibited by the base alloy.

Narayana et al. [15] investigated the corrosion behavior of aluminum–graphene oxide (Al/GO) nanocomposites at various immersion durations, using the immersion corrosion technique. The composites were produced via ultrasonic gravitational stir casting. Results showed that as

immersion time increased, the corrosion rate decreased, but weight loss increased. Additionally, non-immersed samples had higher microhardness than the immersed ones, indicating degradation due to corrosion exposure.

Kvashnichev [16] investigated the corrosion resistance of the Al-Al_2O_3 nanocomposites, produced via a chemical interaction between titanium nanooxide and molten aluminum in molten alkali chlorides at temperatures above 70 °C. X-ray diffraction and electron microscopy confirmed a uniform distribution of α-Al_2O_3 nanoparticles within the aluminum matrix. In comparison to pure aluminum, the corrosion rate in 0.5 M NaCl diminished by 3–4 times, and the corrosion mechanism transitioned from pitting to uniform, elevating the resistance rating from class 3 (resistant) to class 2 (extremely resistant). This enhancement is ascribed to the development of a compact, single-phase hydroxide layer on the composite surface. However, the corrosion potential remained unaffected by the presence of the nanoparticles. The present study focused on evaluating the microstructural features and corrosion resistance of Al alloy A356 in both as-cast form and as an in-situ composite reinforced with 5, 10, and 15 wt% Ni particles in a 3.5% NaCl solution.

This study presented a systematic investigation of the A356/Al_3Ni in-situ composites produced by conventional stir casting with varying Ni contents (5–15 wt.%). Unlike many prior reports that considered only microstructure or only mechanical properties, here the authors concurrently correlated microstructural evolution (Al_3Ni formation and grain refinement), microhardness, and electrochemical corrosion behavior in 3.5 wt.% NaCl. The novelty findings presented are the following:

1. Use of in-situ fabrication by stir casting to form Al_3Ni intermetallic compound within the A356 aluminum alloy matrix.
2. Investigation of varying Ni content (5, 10, and 15 wt%) to study its effect on both hardness and corrosion resistance.
3. Identification of an optimal Ni content (5 wt%) for achieving maximum corrosion resistance, a finding not commonly reported.

EXPERIMENTAL WORK

Materials used and specimen preparation

The current investigation utilized aluminum alloy A356, which was manufactured from a master alloy of Al 11 wt% Si and commercially pure aluminum. These metals are generally supplied to the electrical industry. Each material was melted using an electric resistance furnace, with the furnace temperature set at 750 °C.

The alloy was melted and subsequently poured into a metallic mold after the chemical composition had been adjusted. The chemical structure of the resultant aluminum alloy A356 was ascertained utilizing a Thermo ARL 3460 optical emission spectrometer. The chemical composition of the manufactured Al alloy A356 is detailed in Table 1. Employing A356 as the matrix and micro Ni particles of 1.0175 µm as reinforcement, in-situ Al_3Ni composites were fabricated with varying Ni contents of 5, 10, and 15 wt%.

Aluminum alloy A356 was placed at 750 °C, above the liquidus temperature, into an alumina crucible within an electric furnace. The melt was held at this temperature for approximately 15 minutes to achieve homogenization, after which flux (1% CaF_2) was incorporated to eliminate impurities as slag. Ni particles, wrapped in aluminum foil, were preheated to 350 °C for 1 hour to remove moisture prior to addition. Ni powders were gradually introduced into the molten alloy while stirring at 500 rpm with an electric stirrer to ensure uniform dispersion of the reinforcement and to perform degassing with argon (an inert gas at a flow rate of 2.5 L/min), as it was shown in Figure 1. Subsequently, the melt was poured into a steel mold preheated to 250 °C, with dimensions of 120 mm in height and 15 mm in diameter.

Tests and inspections

Utilizing an optical microscope, the specimens that are made from a cross-section have been examined. Wet grinding was performed with the use of water as well as SiC emery paper in grits of 320, 500, 600, 800, 1000, and 1200.

Table 1. Chemical composition of the prepared A356 alloy

Element (wt%)	Si	Fe	Cu	Mn	Mg	Zn	Ti	Al
Measured value	7.38	0.5	0.2	0.1	0.4	0.3	0.02	Balance
Standard value	6.6–7.5	0.6	0.25	0.35	0.20–0.45	0.35	0.25	Balance

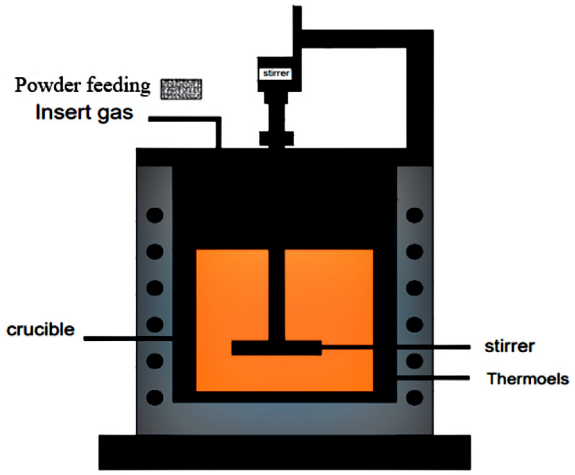

Figure 1. Stir casting system

Diamond paste of 0.50 µm with a specialized cloth for polishing and lubrication was used to polish the samples. The specimens were etched with the use of Keller's reagent etching solution, which is comprised of 95 milliliters of H_2O, 2.50 milliliters of HNO_3, 1.50 milliliters of HCI, and 1 milliliter of HF. After washing, they have been dried. The Vickers hardness test has been performed with the use of a digital micro-hardness tester of the Laryee, Model HVS1000 variety. SEM (Scanning Electron Microscope) equipment, type VEGA3LMe with a high-resolution mode, was used.

Grain size measurement was carried out using Digital Image Analysis: ImageJ, an open-source image processing software widely used for its flexibility and accuracy in evaluating the grain structures from optical microscope images.

In the current study, the average grain size for the base alloy A365 and in-situ composites reinforced with 5, 10, and 15 wt% Ni was measured using the ImageJ program. The X-ray diffraction (XRD) patterns of the specimens were recorded to determine the phases present in the microstructures using a diffractometer (Bruker D8) equipped with Cu-Kα radiation. A computerized microhardness tester (Laryee, Model HVS-1000) was utilized to conduct Vickers hardness testing. A load of 200 grams was imposed for 15 seconds, and a mean of three readings was taken for every specimen at various sites.

To calculate the corrosion rate, the polarization curves of the examined specimens were measured in a solution of 3.5 wt% NaCl was determined. Corrosion experiments were carried out on the top surface of the FSPed specimens employing an Autolab potentio/galvanostat (see Figure 2), with all specimens having the same surface area (1 cm^2). Prior to the tests, the sample surfaces were first polished to achieve a similar roughness and then washed with acetone, after immersing the specimens in a solution of 3.5 wt.% NaCl for 30 min to provide a nearly fixed open-circuit potential (OCP), they were polarized at a 1 mV/s scan rate within a potential range of -200 to +500 mV against the OCP. Calomel and platinum wire were used as reference and counter electrodes, respectively. The Tafel extrapolation method was employed to determine the corrosion current density of the specimens and the corrosion rate employing the subsequent Equation 1:

$$C.R\ (mpy) = 0.13\ icorr\ EW/\rho \qquad (1)$$

where: I_{corr} is the corrosion current (µm/ cm^2), EW is the equivalent weight, ρ is the metal density (gm/cm^3).

RESULTS AND DISCUSSION

Microstructure examination

Optical micrographs

Figure 3 displays the optical micrographs of the cast aluminum alloy A356 and in-situ composites with 5, 10, and 15 wt% Ni. Figure 3a shows that the microstructure of A356 alloy consists of the Al-Si eutectic (dark regions) as well as the α-Al phase (white regions). The α-Al dendrites are surrounded by a continuous phase that is referred to as the eutectic phase. Figures 3b, 3c, and 3d show the microstructure of the in-situ composites with

Figure 2. The potentiostat instrument used for the corrosion test

different contents of Ni (5, 10, and 15 wt%) nickel powders, respectively, which were added to the matrix of the Al alloy A356. The in-situ composite consists of Al_3Ni, an intermetallic compound formed with near uniform distribution in the Al matrix, which also led to changes in the grain size, grain morphology, and phase structure from coarse dendrites to refined and homogenous grains. More Ni powder led to more Al_3Ni, and clusters were seen as expected from Figure 3d Furthermore, it was noticed that the average grain size reduces from 125 μm for the base alloy (see image a) to 85, 65, and 45 μm for 5, 10, and 15 wt% Ni in-situ composites (see Figure 3b–d), respectively. Heterogeneous nucleation: The intermetallic particles of Al_3Ni and Al_3Ni_2 act as potent nucleation sites during solidification, increasing the number of nuclei and reducing the average grain size. Growth restriction: The solute Ni atoms restrict dendritic growth by increasing the growth restriction factor, which limits grain coarsening during solidification that leads to grain refining the microstructure of A356 alloy. Dislocation and grain boundary pinning: The fine dispersion of Al–Ni intermetallics inhibits the grain boundary motion through the Zener pinning effect, further stabilizing the fine-grained structure. These findings align with those of other literature [17–18].

Scanning electron microscope (SEM) examination

The SEM micrographs regarding the base alloy A356, as well as the in situ composites with varying weight percentages of Ni (5, 10, and 15 wt%), respectively, are displayed in Figure 4. Figure 4a displays the SEM morphology of the matrix Al phase and Al-Si eutectic in the alloy A356. Figures 4b and 4c show the SEM micrographs of the in-situ composites with 5 and 10 wt% Ni, respectively. The intermetallic compounds Al_3Ni have almost uniform distribution with some agglomeration in the aluminum matrix. Figure 4d illustrates the dispersion of the Al_3Ni intermetallic complex, highlighting diverse forms and sizes of agglomerations seen in 15 wt% Ni. Furthermore, the grain refinement, particle fragmentation, and distribution within the Al matrix were observed. These results are in agreement with other researchers [19–22].

X-ray diffraction analyses

The XRD diagrams of the base alloy A356 sample and the in-situ composite samples

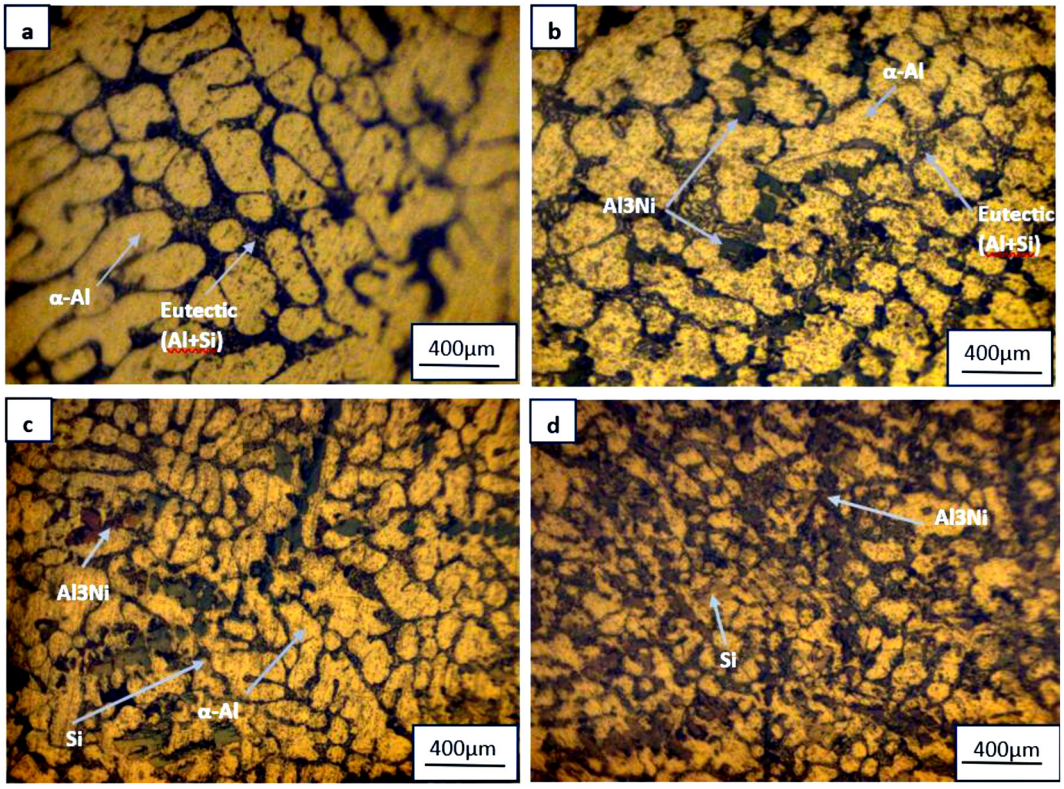

Figure 3. The optical microstructure of: (a) base Al alloy (A356), (b) in-situ composite (A356 – 5% Ni), (c) in-situ composite (A356 – 10% Ni), and (d) in-situ composite (A356 – 15% Ni) at 100x

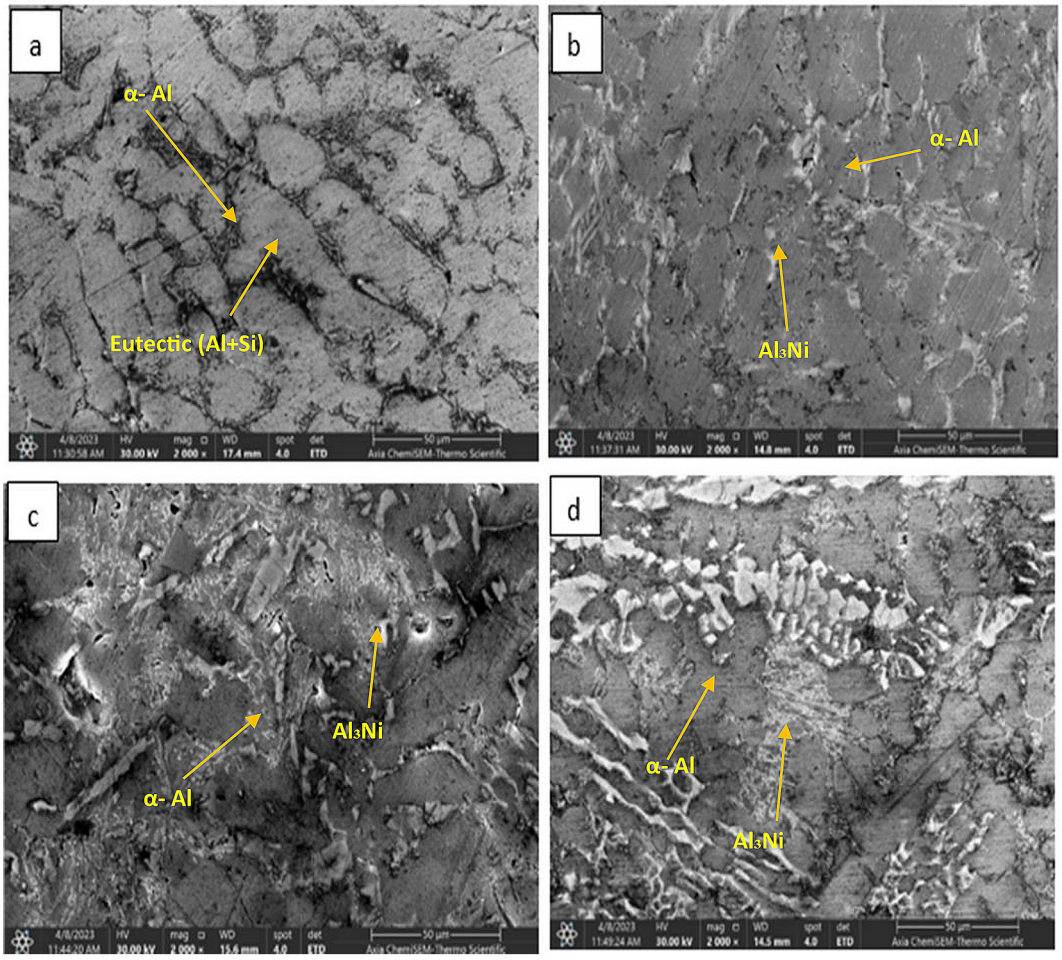

Figure 4. The SEM morphology: (a) as cast Al alloy A356, (b) Al alloy A356 with 5%Ni composite, (c) Al alloy A356 with 10%Ni composite, (d) Al alloy A356 with 15%Ni composite

containing 5, 10, and 15 wt.% Ni are displayed in Figures 5, 6, 7, and 8, respectively. It was found that the presence of the main phases included α-Al, Al_3Mg_2, and Si as peaks in the XRD pattern of A356 alloy and A356 in-situ composite. In contrast, the appearance of peaks corresponding to intermetallic compounds (Al_3Ni and Al_3Ni_2) phases is shown in the XRD pattern of the A356 in-situ composite. The X-ray diffraction results indicated the precipitates of secondary-phase particles Al_3Mg_2 in the a-Al phase and primary Si. It is observed that the peaks for the Al_3Ni and Al_3Ni_2 phases increase along with the Ni content in the in-situ composite. These results are in agreement with the results of other researchers [11,19].

Microhardness results

The results obtained from the microhardness test using the Vickers hardness tester are shown in Table 2. It was seen that the average hardness values regarding the base aluminum alloy and the in-situ composites were 76, 123, 140, and 152 kg/mm², respectively. The findings, which are displayed in Figure 9, show that the hardness values increased along with the weight percentage of Ni. This improvement is because of a greater occurrence of strong interfacial bonds, including the hard intermetallic (Al_3Ni), which are integrated into the soft aluminum matrix and increase the resistance of the material to deformation, thus increasing its hardness.

A distinct and refined interfacial bond is achieved through the exothermic reaction that occurs during the fabrication of in-situ composites. The binary system comprises two solid solutions and five thermodynamically stable intermetallic compounds: Al_3Ni, Al_3Ni_2, Ni_5Al_3, and Ni_3Al, with two phases discovered in these studies [23–24]. Gasparyan and Shteinberg [25] used a custom-designed DTA to illustrate the occurrence of pre-combustion solid-state processes and eutectic

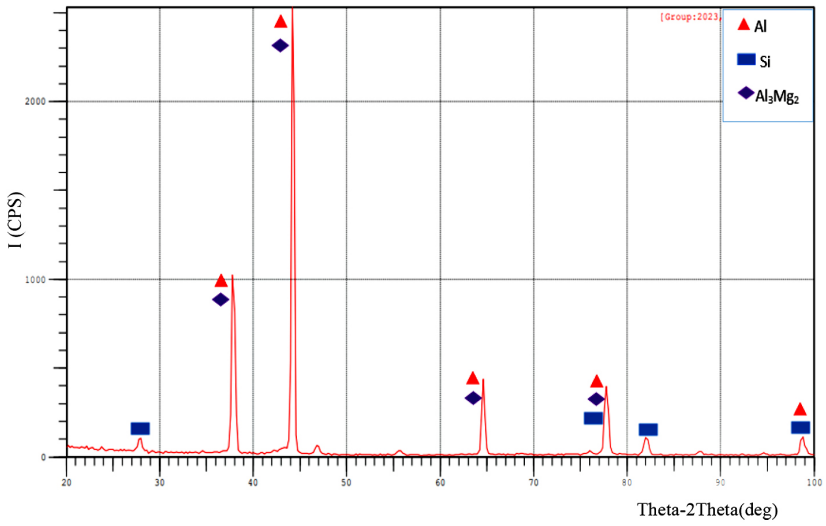

Figure 5. XRD for cast A356 Al alloy

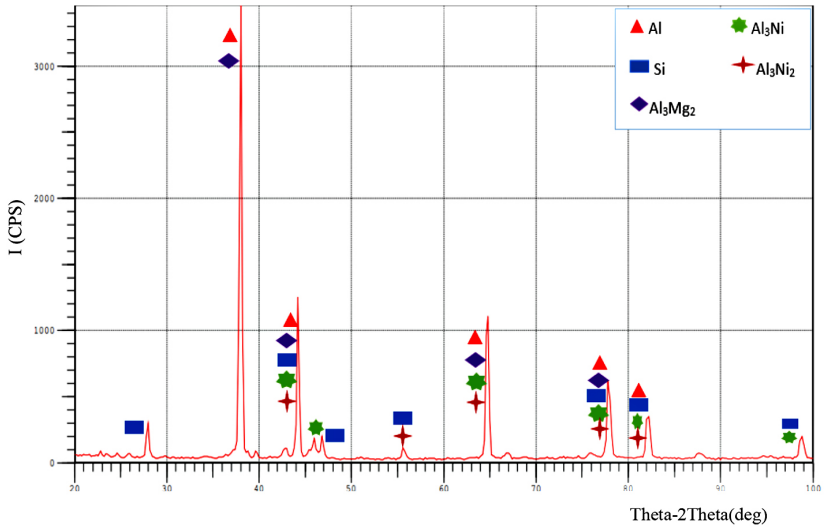

Figure 6. XRD for the in-situ A356-5%Ni composite

melting. Further, they suggested three successive reaction steps leading to the sequential formation of Al_3Ni, Al_3Ni_2, and NiAl. The following equations express the sequence of phase formation:

$$3Al + Ni \rightarrow Al_3Ni + 258\ kcal/mol \quad (1)$$

$$Al_3Ni + Ni \rightarrow Al_3Ni_2 + 90\ kcal/mol \quad (2)$$

$$Al_3Ni_2 + Ni \rightarrow 3NiAl + 212\ kcal/mol \quad (3)$$

The interaction between aluminum and nickel is exothermic, resulting in the formation of a Al_3Ni phase that develops as a spherical shell at the Ni–Al contact, as described by Equation 1. Therefore, the hardness of the composite is greatly enhanced by the soundness of the casting and the prepared method by stir casting. Chandrashekar [13] has noted that the hardness increased along with the concentration of the in-situ composite.

Corrosion results

Figure 10 (a–e) displays the Tafel extrapolation polarization curves of all the samples exposed to the solution of 3.5 wt% NaCl. The potentiodynamic polarization curves were used to derive several electrochemical parameters, which are listed in Table 3. These electrochemical parameters include the corrosion potential (Ecorr), corrosion current (Icorr), anodic Tafel slope (βa), cathodic Tafel slope (βc), and corrosion rate (mpy) for both the base sample and the in-situ composite samples. All of the sample polarization curves manifested a

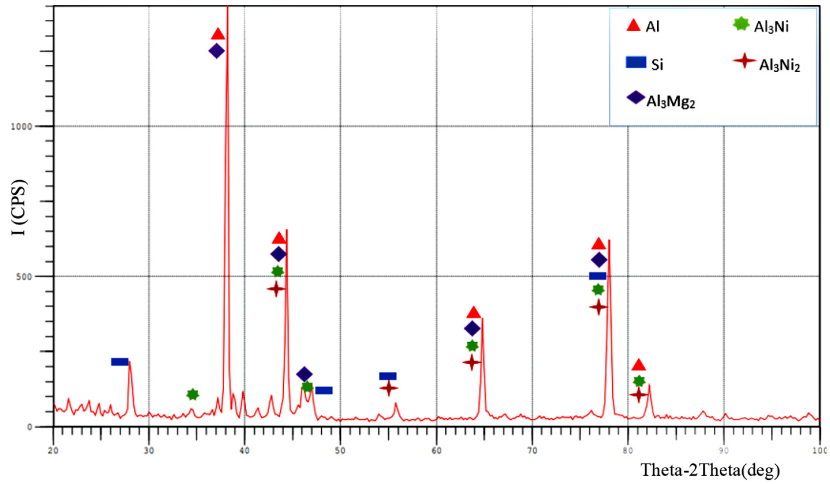

Figure 7. XRD for the in-situ A356-10%Ni composite

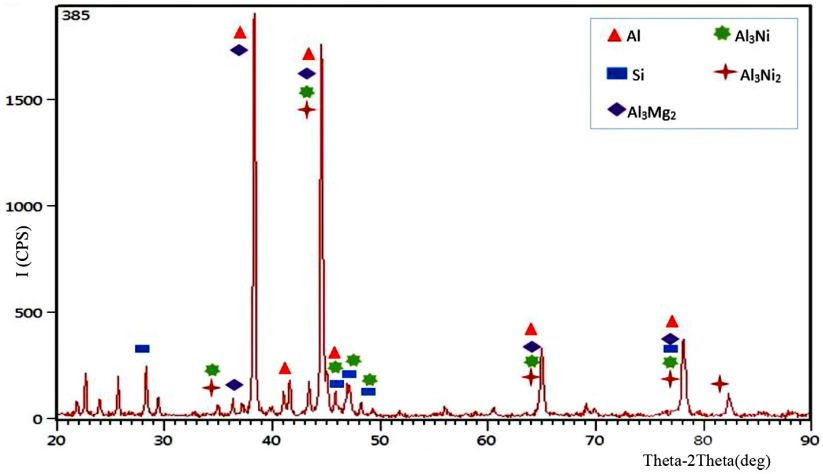

Figure 8. XRD for the in-situ A356-15%Ni composite

Table 2. Mechanical properties of Al alloy A356 and in-situ composites

Symbol	Specimens	Microhardness (HV) Kg/mm²	Improvement%
A	As cast Al alloy A356	76	–
B	Al alloy A356 with 5%Ni	123	61%
C	Al alloy A356 with 10%Ni composite	140	84%
D	Al alloy A356 with 15%Ni composite	152	100%

clear difference. The difference is due to the role of the intermetallic compound Ni_3Al in-situ particles acting as a filling agent in voids, porosity, and pits created during exposure of the sample surface to the corrosive medium [26]. Additionally, these particles of Al_3Ni have higher hardness than that of the A356 matrix, and they act as grain refiners to the a-aluminum matrix and Al-Si eutectic, leading to an increase in the corrosion resistance of in-situ composite samples.

Uhlig and Revie [27] found that minor impurity levels influence the corrosion behavior of aluminum in the metal; all contaminants, except for magnesium, are generally cathodic to aluminum. According to Table 3, the composite containing nanoparticles has a lower corrosion current density, as well as a lower negative potential (making it more noble) than the base metal. This difference is owing to the decreased content of reinforcement in the same alloy matrix, which limits the

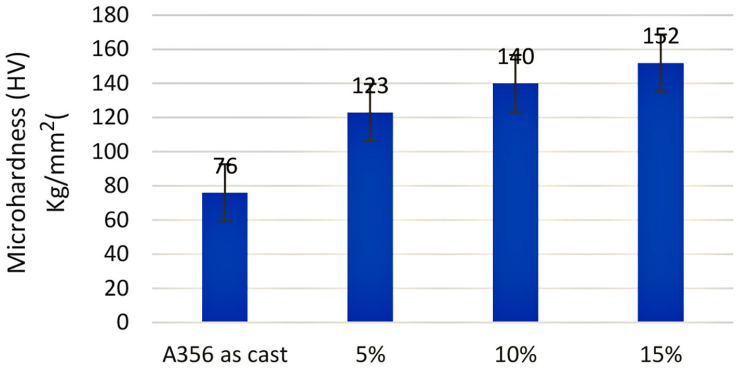

Figure 9. Hardness of the in-situ composites and as-cast A 356 alloy

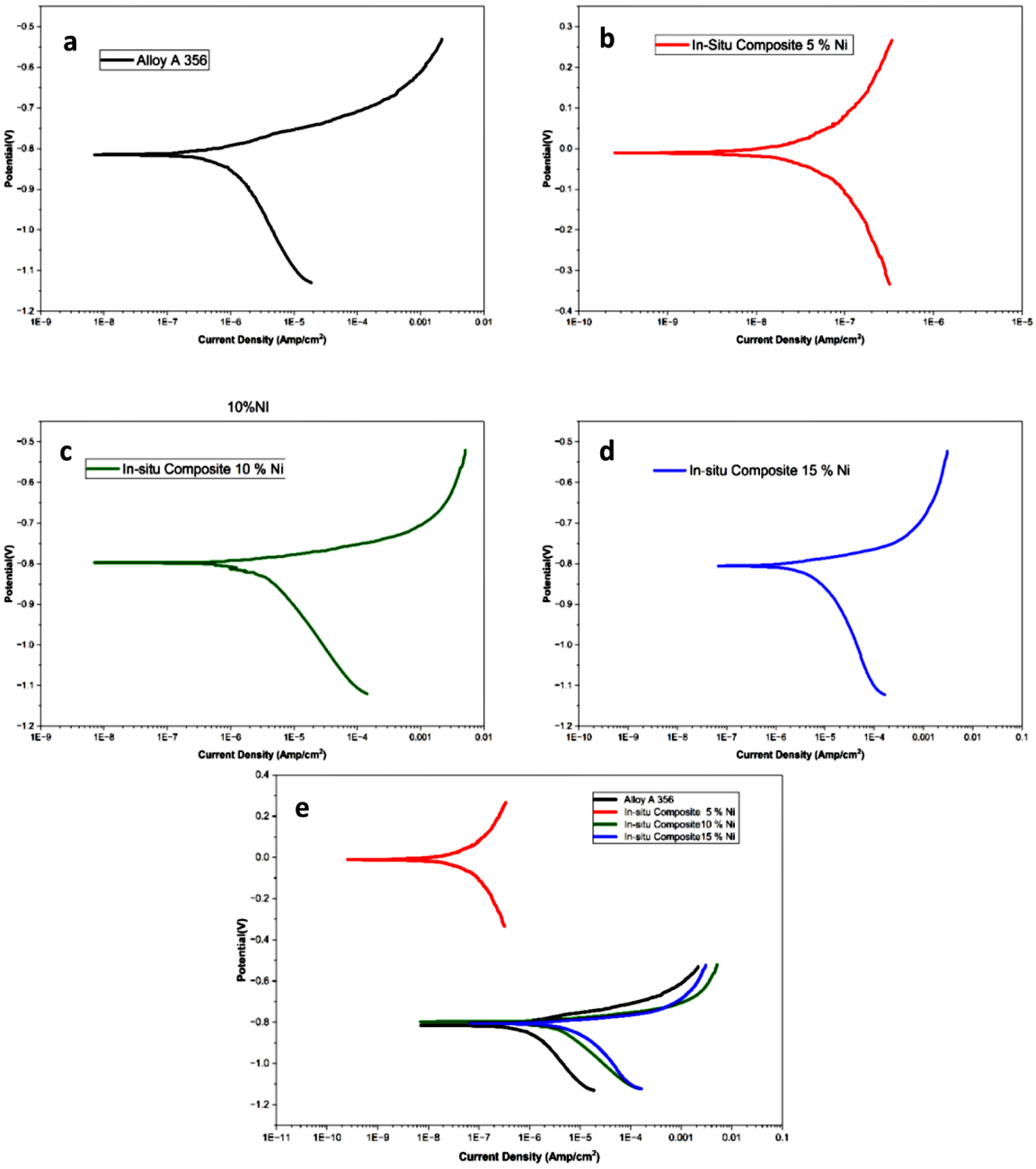

Figure 10. Tafel polarization curves for the base alloy A356 as cast and in-situ composite in (3.5%) NaCl solution (base alloy, 5% Ni, 10% Ni, and 15% Ni)

cathodic areas to the reinforcements, impurities, and porosities in the alloy matrix. Additionally, the remaining stresses in the matrix caused by differences in thermal and mechanical characteristics between the reinforcement and the matrix are regarded as ideal locations for dissolution as well as pitting [28]. Such findings are consistent with those of other studies [29].

Table 3 presents the electrochemical corrosion behavior of various A356 alloy specimens, including the as-cast condition and in-situ composites reinforced with different weight percentages of Ni nanoparticles, all immersed in a 3.5 wt% NaCl solution.

Corrosion current density (Icorr) and corrosion potential (Ecorr)

The A356 in-situ composite with 5% Ni exhibited the lowest corrosion current (8.8457×10^{-9} A), indicating the highest corrosion resistance among all specimens. The improvement in corrosion resistance was 97%. This enhancement can be attributed to the development of thicker and more consistent protective oxide layers on the alloy surface [30]. It exhibited a significantly lower corrosion potential (-0.01051 V), which suggests more noble behavior. In contrast, the as-cast A356 sample recorded the highest corrosion current (2.9184×10^{-6} A), implying the poorest corrosion resistance due to the absence of reinforcement. As the Ni content increased to 10% and 15%, the corrosion current also increased to 8.5287×10^{-7} A and 1.9052×10^{-6} A, respectively, suggesting a deterioration in corrosion resistance at higher reinforcement levels [31].

Corrosion rate (mpy)

The 5% Ni-reinforced composite achieved the lowest corrosion rate (0.0001 mpy), indicating a significant improvement compared to the as-cast specimen (0.0034 mpy). This improvement was attributed to the effective distribution of nanoparticles, which reduces the cathodic sites and improves the structural characteristics of the matrix. However, when the Ni content was increased to 10% and 15%, the corrosion rate increased to 0.0100 mpy and 0.0225 mpy, respectively. The increase was suggested to be due to particle agglomeration or the creation of localized galvanic cells, promoting pitting corrosion [32].

Cathodic and anodic tafel slopes (βc and βa)

A slight decrease in the ßc values from 67.791 to 60.03 was observed, indicating changes in the cathodic reaction mechanism. The ßa value increased with 5% Ni reinforcement (50.783) and then decreased at higher Ni contents, possibly reflecting a shift in the anodic dissolution mechanism or increased susceptibility to localized attack. These results were confirmed by Muna and Basma [26]. The cyclic polarization curves presented in Figure 11 further illustrate the corrosion performance of the specimens. The curve of the as-cast alloy exhibited a steep rise in current density at lower potentials, indicative of active corrosion and a tendency toward localized attacks, such as pitting. The 5% Ni composite, however, exhibits the most favorable behavior, with a wide passive region and low current density, suggesting strong passivation and improved stability of the protective oxide layer. On the other hand, the specimens with 10% and 15% Ni exhibit higher current densities and narrower passive regions, indicating weaker passivation and increased susceptibility to breakdown. These shifts suggest that excessive reinforcement compromises the protective effect, likely due to the presence of surface defects or poorly dispersed particles.

The data from both Table 3 and Figure 11 consistently demonstrate that a reinforcement content of 5% Ni achieves the most effective enhancement in corrosion resistance. Beyond this level, the corrosion behavior worsens, highlighting the critical importance of optimizing the amount and distribution of reinforcement particles in metal

Table 3. Electrochemical corrosion outcomes of the specimens that are immersed in a 3.5% NaCl solution

ITEM	OCP (volt)	E corr. (volt)	I corr. (Amp.)	Corr. rate (mpy)	βc	βa	Improvement % In C.R
A356 as cast	-0.8296	-0.81497	2.9184×10^{-7}	0.0034	67.791	40.054	–
A356 in-situ composite (5%Ni)	-0.7880	-0.01051	8.8457×10^{-9}	0.0001	60.03	50.783	97%
A356 in-situ composite (10%Ni)	-0.1575	-0.79695	8.5287×10^{-7}	0.0100	65.698	20.311	–
A356 in-situ composite (15%Ni)	-0.8395	-0.80518	1.9052×10^{-6}	0.0223	64.64	24.228	-

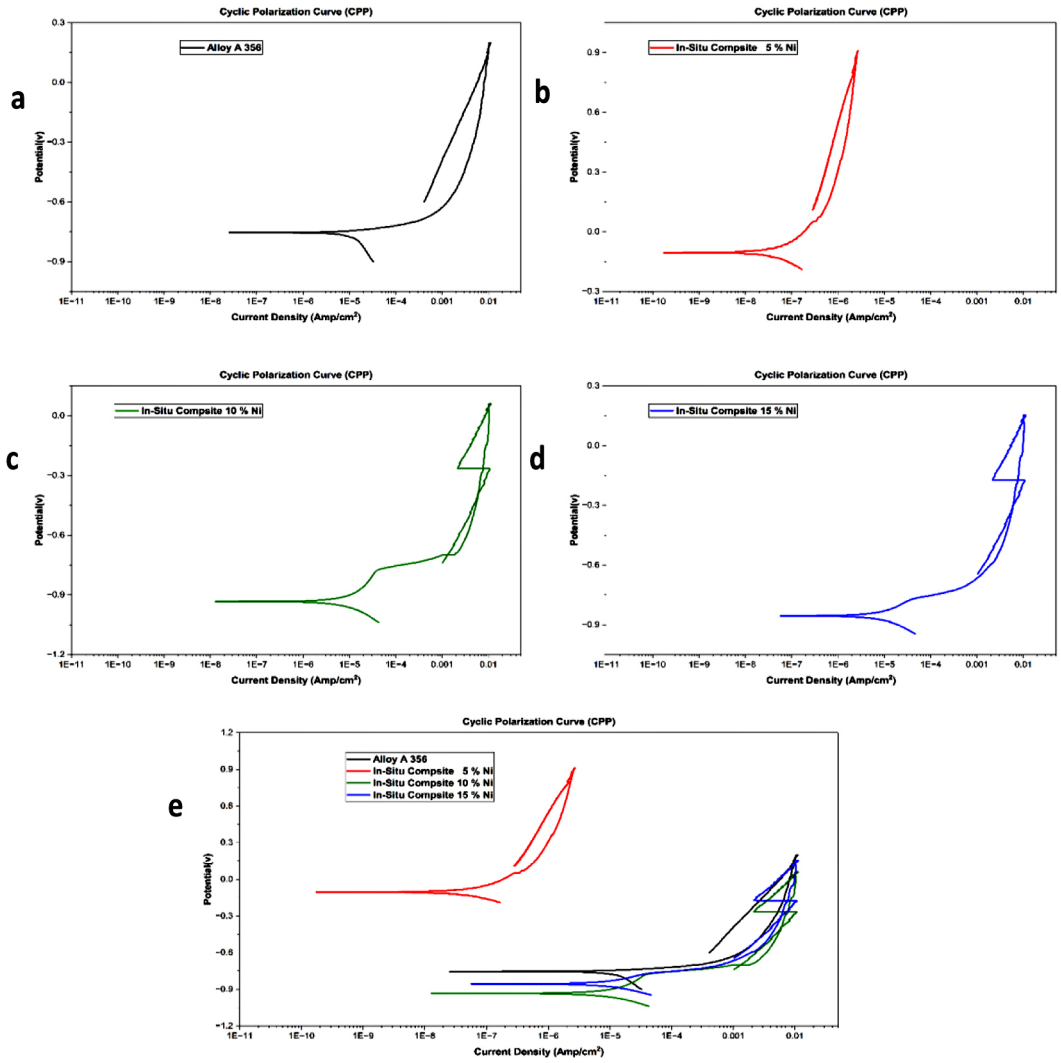

Figure 11. Cyclic polarization curves for the base alloy A356 as cast and in-situ composite in (3.5%) NaCl solution

matrix composites. These results are in agreement with those of researchers [33].

Also, the base specimen exhibits the uppermost corrosion vulnerability; however, after the surface treatment with FSP, further improvement in the resistance to corrosion was observed when the tool traverse speed was increased. The fact that numerous studies have shown a clear correlation between the produced passive film and the size of the grain, as well as the resistance of the alloy to corrosion in aluminum, should be stressed. It is anticipated that a decrease in the size of the grain will cause a significant shift in the electrochemical conductivity due to the distinct characteristics of grain boundaries in comparison to the bulk substances, such as reactivity, rates of diffusion, and atomic coordination [34]. Another effect of grain refining is the breakdown of the intermetallic phases. Due to the cathodic character of these intermetallic compounds in relation to the aluminum matrix, their dissolution and refinement will significantly increase the corrosion resistance. Such outcomes are in agreement with those of other investigators [35–36].

Micrograph characterization results after corrosion test

Figure 12 illustrates the damaged surface subsequent to the corrosion test of A356 as-cast and in-situ composites in a 3.5% NaCl solution. The A356 as-cast and in-situ composite underwent pitting corrosion. Figure 12a illustrates extensive high-intensity pits distributed throughout a substantial region of the matrix alloy. These trenches seem to be increased in both size and depth. In Figure 12b, the pits of the in-situ composite with 5 wt% Ni appear fine and small, with fewer pits compared with the

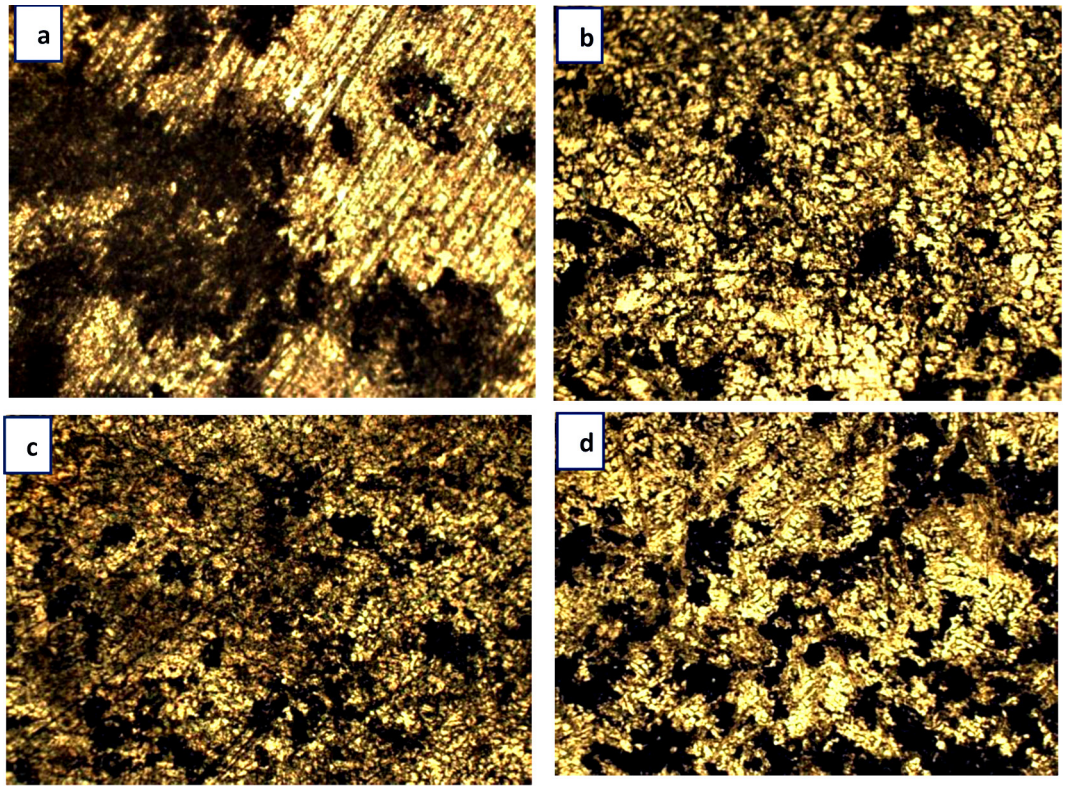

Figure 12. Optical micrographs show the corroded surface (a) base Al alloy (A356), (b) in-situ composite (A356 – 5%Ni), (c) in-situ composite (A356 – 10% Ni), (d) in-situ composite (A356 – 15% Ni)

images in Figures 12c and 12d. Furthermore, it is obvious that the in situ composite with 10 wt% and 15 wt% Ni was subjected to more severe corrosion, as shown in Figure 12c compared with Figure 12b, where severe attack was obvious. These findings agree with the results [37,38].

Comparison with recent literature and mechanistic interpretation. The pronounced improvement of corrosion resistance observed for the 5 wt.% Ni composite in the conducted study is consistent with recent reports that small, well-dispersed Al_3Ni precipitates can promote uniform passive film formation and reduce effective cathodic sites on Al-Si matrices. For example, Román et al. [39] observed localized corrosion adjacent to Al_3Ni precipitates at high Ni contents and noted improved uniformity at lower Ni levels, supporting the authors' own conclusion that low Ni additions improve passivation. Conversely, the deterioration of corrosion performance at 10–15 wt.% Ni in the samples studied in this paper can be explained by particle agglomeration and the formation of local galvanic couples (Al matrix vs. Ni-rich intermetallics) that act as initiation sites for pitting.

Mechanistically, grain refinement (observed here with increasing Al_3Ni) tends to increase the density of grain boundaries which can either enhance passive film formation (beneficial) or provide fast diffusion paths for aggressive species depending on particle distribution; Therefore, the obtained results emphasize that an optimal, low Ni fraction (≈5 wt.%) provides the best trade-off – sufficient Al_3Ni to refine grains and harden the matrix while avoiding the adverse agglomeration and galvanic effects that become dominant at higher Ni contents.

CONCLUSIONS

The results obtained in this study on the effect of adding different amounts 5, 10, and 15 wt% of Ni to the A356 alloy on microstructure and corrosion properties are as follows:

- It was shown that the stir casting technique successfully produced the in-situ composites (A356/Al_3Ni) with the addition of various Ni contents to the base alloy A356.
- The stir casting method used in the preparation of the in-situ composites reinforced with 15 wt% Ni enhanced the grain refinement from the base alloy 125 μm to 45 μm in the 15 wt% Ni composite, as well as particle

fragmentation and distribution within the Al matrix, due to dislocation-pinning effects.

- The microhardness improvement of the in-situ composite increased by 61%, 84%, and 100%, respectively, at 5, 10, and 15 wt% Ni compared to the base alloy A356.
- From Tafel polarization results, it was found that the corrosion resistance improved with the addition of 5 wt% Ni particles (97% improvement). In contrast, the in-situ composites with 10 wt% Ni and 15 wt% Ni showed lower corrosion resistance than that of the composite with 5 wt% Ni and the base alloy A356 in a 3.5% NaCl solution.
- It was noticed that the base alloy and composite samples containing 10 wt% Ni and 15 wt% Ni had similar anodic polarization curves and showed repassivation potentials. In comparison, the in-situ composite containing 5 wt% Ni and the base alloy A356 exhibited less susceptibility to pitting corrosion in a 3.5% NaCl solution.
- The present work demonstrates that a careful balance of the Ni content in the A356/Al_3Ni in-situ composites allows tailoring between mechanical strengthening and corrosion performance: ~5 wt.% Ni yields optimum corrosion resistance in 3.5 wt.% NaCl, while 15 wt.% Ni maximizes hardness.

REFERENCES

1. Shamanian M, Bahrami E, Edris H, et al. Fabrication of in situ nickel intermetallic compound dispersed aluminum matrix composites by friction stir process. Surface Review and Letters. 2018;25(7):1950010. https://doi.org/10.1142/S0218625X19500100
2. Ervina Efzan MN, Siti Syazwani N, Al Bakri AMM. Fabrication method of aluminum matrix composite (AMCs): A review. Key Engineering Materials. 2016;700(1):102–10. https://doi.org/10.4028/www.scientific.net/KEM.700.102
3. Abbass MK. Effect of Cd on microstructure and dry sliding wear behavior of (Al-12% Si) alloy. The journal of engineering research. 2010;7(1):1–10. https://doi.org/10.24200/tjer.vol7iss1pp1-10
4. Alam MT, Ansari AH. Ceramic materials and stir cast aluminium matrix composites: A literature review. International Journal of Innovative Research in Science, Engineering and Technology. 2017;6(7):14148–60. http://dx.doi.org/10.15680/IJIRSET.2017.0607201
5. Sijo MT, Jayadevan KR. Analysis of stir cast aluminium silicon carbide metal matrix composite: A comprehensive review. Procedia Technology. 2016;24(1):379–85. https://doi.org/10.1016/j.protcy.2016.05.052
6. Shivalingaiah K, Nagarajaiah V, Selvan CP, et al. Stir casting process analysis and optimization for better properties in Al-MWCNT-GR-based hybrid composites. Metals. 2022; 12(8): 1297. https://doi.org/10.3390/met12081297
7. Aynalem GF. Processing methods and mechanical properties of aluminium matrix composites. Advances in Materials Science and Engineering. 2020; 2020(1): 3765791. https://doi.org/10.1155/2020/3765791
8. Essien UA, Vaudreuil S. In-situ metal matrix composites development for additive manufacturing: A perspective. Journal of Achievements in Materials and Manufacturing Engineering. 2022;111(2):78–85. http://dx.doi.org/10.5604/01.3001.0015.9997
9. Viet NH, Oanh NTH. Microstructure and electrical property of ex-situ and in-situ copper titanium carbide nanocomposites. Metals. 2020;10(6):735. https://doi.org/10.3390/met10060735
10. Gobalakrishnan B, Rajaravi C, Udhayakumar G, et al. Effect of ceramic particulate addition on aluminium based ex-situ and in-situ formed metal matrix composites. Metals and Materials International. 2021; 27(9): 3695–708. https://doi.org/10.1007/s12540-020-00868-6
11. Gong YP, Ma SM, Hei HJ, et al. Tailoring microstructure and its effect on wear behavior of an Al–7Si alloy reinforced with in situ formed Al3Ti particulates. Journal of Materials Research and Technology. 2020;9(4):7136–48. https://doi.org/10.1016/j.jmrt.2020.04.061
12. Abu-Warda N, López MD, Escalera-Rodríguez MD, et al. Corrosion behavior of mechanically alloyed A6005 aluminum alloy composite reinforced with TiB_2 nanoparticles. Materials and Corrosion. 2020; 71(3): 382–91. https://doi.org/10.1002/maco.201911174
13. Chandrashekar J, Annaiah M, Chandrashekar R. Microstructure and mechanical properties of aluminum cast alloy A356 reinforced with dual-size B4C particles. Fracture and Structural Integrity. 2021;15(57):127–37. https://doi.org/10.3221/IGF-ESIS.57.11
14. Dawood NM, Hassan AA. Corrosion Behavior of Al-Ni matrix composites in a dilute sodium chloride solution. Technology Reports of Kansai University. 2021;63(3):7439–48.
15. Narayanan S, Sozhamannan GG, Hemalatha K, et al. Corrosion and hardness behaviour of AL/GO nanocomposites processed by the ultrasonic gravitational stir casting method. International Journal of Corrosion. 2021;2021(1):6658186. https://doi.org/10.1155/2021/6658186
16. Kvashnichev AG, Yolshina LA, Pryakhina VI. Corrosion-electrochemical behavior of Al–Nano–Al_2O_3 metal matrix composites in an aqueous 0.5 M NaCl solution. Russian Metallurgy (Metally). 2024;2024(1):225–32. https://doi.org/10.1134/S0036029524701568
17. Baheer NA, Abbass MK, Aziz IAA-K. Effect of friction stir processing on microstructure and mechanical properties of in-situ composite A356/

Al3Ni fabricated by stir casting. International Journal of Computational Methods and Experimental Measurements. 2024;12(4):453–61. https://doi.org/10.18280/ijcmem.120414

18. Fouad MJ, Abbass MK, İnanç İ. Manufacture of self-lubricating mechanical parts from Al-Si alloy matrix hybrid nanocomposites. Tribology in Industry. 2025;47(1):112–24. http://dx.doi.org/10.24874/ti.1752.09.24.02
19. Liu S, Paidar M, Mehrez S, et al. Fabrication of AA6061/316 composites via a double pin FSP tool. Journal of Materials Research and Technology. 2022;20(9):2826–40. https://doi.org/10.1016/j.jmrt.2022.07.156
20. Matsumuro M, Kitsudo T. Fabrication of in-situ intermetallic compound dispersed aluminum matrix composites by addition of metal powders. Materials Transactions. 2006;47(12):2972–9. https://doi.org/10.2320/matertrans.47.2972
21. Ma S, Wang Y, Wang X. The in-situ formation of Al_3Ti reinforcing particulates in an Al-7wt%Si alloy and their effects on mechanical properties. Journal of Alloys and Compounds. 2019;792(7):365–74. https://doi.org/10.1016/j.jallcom.2019.04.064
22. Kargul M, Borowiecka-Jamrozek JM. Fabrication and characteristics of cast aluminium – mineral particles composite. Advances in Science and Technology Research Journal. 2024;18(5):75–89. https://doi.org/10.12913/22998624/190073
23. Dhanasekaran R, Kumar KS. Microstructure, mechanical properties of A356/Li aluminum alloy fabrication by stir casting method. International Journal of Applied Engineering Research. 2015;10(50):416–9.
24. Kaviyarasan K, Thiyagu S, Shabari V, et al. Investigation on mechanical properties of aluminium alloy A356 by reinforcing with TiB2 & WC composites. IOP Conference Series: Materials Science and Engineering. 2021;1145(1):012110. https://doi.org/10.1088/1757-899X/1145/1/012229
25. Gasparyan AG, Shteinberg AS. Macrokinetics of reaction and thermal explosion in Ni and Al powder mixtures. Combustion, Explosion and Shock Waves. 1988;24(3):324–30. https://doi.org/10.1007/BF00750616
26. Abbass MK, Sultan BF. Influence of Al2O3 and SiO2 nano-particles on hardness and corrosion resistance of aluminum alloy (Al-4.5%Cu-1.5%Mg). Materials Research Express. 2019;6(10):1050a8. https://doi.org/10.1088/2053-1591/ab4066
27. Revie RW, Uhlig HH. Corrosion and Corrosion Control: An Introduction to Corrosion Science and Engineering. New Jersey: John Wiley & Sons, Inc.; 2008.
28. Nunes PCR, Ramanathan LV. Corrosion behavior of alumina-aluminum and silicon carbide-aluminum metal-matrix composites. Corrosion. 1995; 51(8): 610–7. https://doi.org/10.5006/1.3293621
29. Abbass MK, Hassan KS, Alwan AS. Study of corrosion resistance of aluminum alloy 6061/SiC composites in 3.5% NaCl solution. International Journal of Materials, Mechanics and Manufacturing. 2015;3(1):31–5. https://doi.org/10.7763/IJMMM.2015.V3.161
30. Nabhan Baydaa J, Ghalib L, Jasem Manal H. Evaluation of corrosion resistance of aluminium-silicon carbide composites for thermal application. Corrosion Science and Technology. 2025;24(3):175–83. https://doi.org/10.14773/CST.2025.24.3.175
31. Prathap Singh S, Ananthapadmanaban D, Elil Raja D, et al. Investigating the microstructure, tensile strength, and acidic corrosion behaviour of liquid metal stir casted aluminium-silicon carbide composite. Advances in Materials Science and Engineering. 2023;2023(1):2131077. https://doi.org/10.1155/2023/2131077
32. El-Aziz KA, Saber D, Sallam HE-DM. Wear and corrosion behavior of Al–Si matrix composite reinforced with alumina. Journal of Bio- and Tribo-Corrosion. 2015;1(1):5. https://doi.org/10.1007/s40735-014-0005-5
33. Hussein HA, Kahdim MJ, Atiyah AA. Effects of New Modification and Refinement Techniques of Mechanical Properties and Corrosion Behaviours of Al-Si Alloys. IOP Conference Series: Materials Science and Engineering. 2020;987(1):012014. https://doi.org/10.1088/1757-899X/987/1/012014
34. Abbass MK, Baheer NA. Effect of SiC particles on microstructure and wear behavior of AA6061-T6 aluminum alloy surface composite fabricated by friction stir processing. IOP Conference Series: Materials Science and Engineering. 2020;671(1):012159. https://doi.org/10.1088/1757-899X/671/1/012159
35. Ehsani R, Reihani S. Aging behavior and tensile properties of squeeze cast AL 6061/SIC metal matrix composites. Scientia Iranica. 2004;11(4):392–7.
36. Waheed MS, Abbass MK, Faris AS. Study of corrosion behavior of metal matrix composite based on Al-alloy (7020) prepared by atomization. Engineering and Technology Journal.28(8):1502–13. https://doi.org/10.30684/etj.28.8.1
37. Abbass MK, Hassan KS, Ameen KA. Effect of magnesium addition on corrosion resistance of aluminum -17%silicon alloy. Al-Khwarizmi Engineering Journal. 2017;12(4):50–8. https://doi.org/10.22153/kej.2016.05.003
38. Zamel HH, Salih A-E, Abbass MK, et al. Fabrication of AZ31/ZnO surface composite by friction stir processing: Evolution of microstructure, mechanical properties and corrosion behavior. Advances in Science & Technology Research Journal. 2025;19(5):213–23. https://doi.org/10.12913/22998624/202274
39. Román AS, Ibañez ER, Zadorozne NS, et al. Corrosion susceptibility and microhardness of Al-Ni alloys with different grain structures. Applied Sciences. 2024;14(19):8862. https://doi.org/10.3390/app14198862